SANDIA REPORT
SAND2013-8199
Unlimited Release
Printed September 2013

Genomics-Enabled Sensor Platform for Rapid Detection of Viruses Related to Disease Outbreak

Susan M. Brozik, Ronald P. Manginell, Matthew W. Moorman, Xiaoyin Xiao, Thayne L. Edwards, John M. Anderson, Kent B. Pfeifer, Darren W. Branch, David R. Wheeler, Ronen Polsky, and DeAnna M. Lopez.

Gregory D. Ebel and Abhishek N. Prasad
James A. Brozik, Angela R. Rudolph, and Lillian P. Wong

Prepared by
Sandia National Laboratories
Albuquerque, New Mexico 87185 and Livermore, California 94550

Sandia National Laboratories is a multi-program laboratory managed and operated by Sandia Corporation, a wholly owned subsidiary of Lockheed Martin Corporation, for the U.S. Department of Energy's National Nuclear Security Administration under contract DE-AC04-94AL85000.

Issued by Sandia National Laboratories, operated for the United States Department of Energy by Sandia Corporation.

Available to DOE and DOE contractors from
U.S. Department of Energy
Office of Scientific and Technical Information
P.O. Box 62
Oak Ridge, TN 37831

Telephone: (865) 576-8401
Facsimile: (865) 576-5728
E-Mail: reports@adonis.osti.gov
Online ordering: http://www.osti.gov/bridge

Available to the public from
U.S. Department of Commerce
National Technical Information Service
5285 Port Royal Rd.
Springfield, VA 22161

Telephone: (800) 553-6847
Facsimile: (703) 605-6900
E-Mail: orders@ntis.fedworld.gov
Online order: http://www.ntis.gov/help/ordermethods.asp?loc=7-4-0#online

SAND2013-8199
Unlimited Release
Printed September 2013

Genomics-Enabled Sensor Platform for Rapid Detection of Viruses Related to Disease Outbreak

Susan M. Brozik, Ronald P. Manginell, Matthew W. Moorman, Xiaoyin Xiao, Thayne L. Edwards, John M. Anderson, Kent B. Pfeifer, Darren W. Branch, David R. Wheeler, Ronen Polsky, and DeAnna M. Lopez.

Sandia National Laboratories
P.O. Box 5800

Gregory D. Ebel and Abhishek N. Prasad, Colorado State University
James A. Brozik, Angela R. Rudolph, and Lillian P. Wong, Washington State University

ABSTRACT

Bioweapons and emerging infectious diseases pose growing threats to our national security. Both natural disease outbreak and outbreaks due to a bioterrorist attack are a challenge to detect, taking days after the outbreak to identify since most outbreaks are only recognized through reportable diseases by health departments and reports of unusual diseases by clinicians. In recent decades, arthropod-borne viruses (arboviruses) have emerged as some of the most significant threats to human health. They emerge, often unexpectedly, from cryptic transmission foci causing localized outbreaks that can rapidly spread to multiple continents due to increased human travel and trade. Currently, diagnosis of acute infections requires amplification of viral nucleic acids, which can be costly, highly specific, technically challenging and time consuming. No diagnostic devices suitable for use at the bedside or in an outbreak setting currently exist. The original goals of this project were to 1) develop two highly sensitive and specific diagnostic assays for detecting RNA from a wide range of arboviruses; one based on an electrochemical approach and the other a fluorescent

based assay and 2) develop prototype microfluidic diagnostic platforms for preclinical and field testing that utilize the assays developed in goal 1. We generated and characterized suitable primers for West Nile Virus RNA detection. Both optical and electrochemical transduction technologies were developed for DNA-RNA hybridization detection and were implemented in microfluidic diagnostic sensing platforms that were developed in this project.

ACKNOWLEDGMENTS

This work was funded under LDRD Project Number151324 and Title "Genomics-Enabled Sensor Platform for Rapid Detection of Viruses Related to Disease Outbreak".

CONTENTS

1. Electrocatalytic Detection of Viral RNA Fragments from West Nile Virus

1.1. INTRODUCTION

Nucleic acid hybridization is a fundamental method of molecular biology and plays a central role in diagnostics. Owing to its high specificity, robustness, and the nature of negatively charged duplex structures, a wide range of mechanic, optical, electrical, and electrochemical signal transduction technologies has been implemented into DNA analysis and detection.[1,2,3,4,5] Among those, electrochemical methods are simple, sensitive, cost effective, and rapid. Four DNA bases can be oxidized separately at their respective potentials, but their complete oxidation requires electrode potentials as positive as that for water oxidation, thus challenges the stability of the supporting electrodes that may be oxidized resulting in huge background currents. Among the four bases, guanine oxidation occurs at the least positive potential, which is close to the redox potential of $Ru(bpy)_3Cl_2$.[6,7,8,9], and has become a useful means for DNA assays. DNA-hybridization mediated charge transport has also proven to be a promising DNA sensing mechanism, when it is combined with catalysts, such as gold nanoparticles, redox proteins, and enzymes.[10,11,12,13] Through a catalytic cycle, the enormous amplification improves the on-off signal ratio before and after DNA hybridization, thus, increasing the detection sensitivity dramatically.

We report here a novel surface process to immobilize high density, inosine substituted DNA probes to detect viral RNA (vRNA) fragments derived from West Nile virus. A very similar strategy was reported by Thorp's group using direct adsorption or self-assembled phosphonate monolayers to detect DNA on indium doped tin oxide (ITO) electrodes.[14,15,16] Compared to phosphonic acid, silane modification is more robust. In addition, the carboxylic acid terminal in 11-phosphonoundecanoic acid (UPA) is also well-known to bind ITO electrodes effectively,[17,18] which would lead to low density of free carboxylic acid at the surface for further cross linking with DNA probes.

1.2. MATERIALS, METHODS, AND RESULTS

ITO electrode modification for DNA probe attachment. We applied two separate steps to modify ITO surfaces with high density of free carboxylic acid groups: 1) modify the ITO electrodes with free amines using 3-aminopropyldimethyl-ethoxylsilane or 3-aminopropylmethy-

diethoxylsilane, 2) react the free amines from the surface with 4,4′-Oxydiphthalic anhydride. After these two steps, the ITO electrodes are not only hydrophilic (contact angle < 20°), but also provide higher density of carboxylic acid functionality to covalently attach DNA probes through EDC/NHS reactions. In some cases we modified the ITO electrodes with UPA. Figure 1A illustrates both surface chemistries for probe attachment and catalytic cycle of guanine oxidation by $Ru(bpy)_3Cl_2$. Figure 1B shows much larger catalytic current on silane modified ITOs than surfsces modified by UPA monolayer. The increased peak current or the oxidation charge suggests that the DNA probe density has been increased by ~100%.

Interestingly, we found that EDC, the dehydration catalyst, is essential for covalent peptide bond formation between carboxylate terminated surface and amine-ended DNA probes. In the absence of EDC/NHS, the catalytic oxidation current is almost negligible (red in Figure 1C). The results indicated that both anhydrides in 4,4′-Oxydiphthalic anhydride molecules are reactive to the amines at the surface, and none was left for further reaction with amine-terminated probes. Therefore, two free carboxylic acids are produced from each molecule, leading to higher density of hydrophilic terminals. Such an arching structure also provides higher electron tunneling rate and stability as can be seen from the negative shift of the oxidation potential.

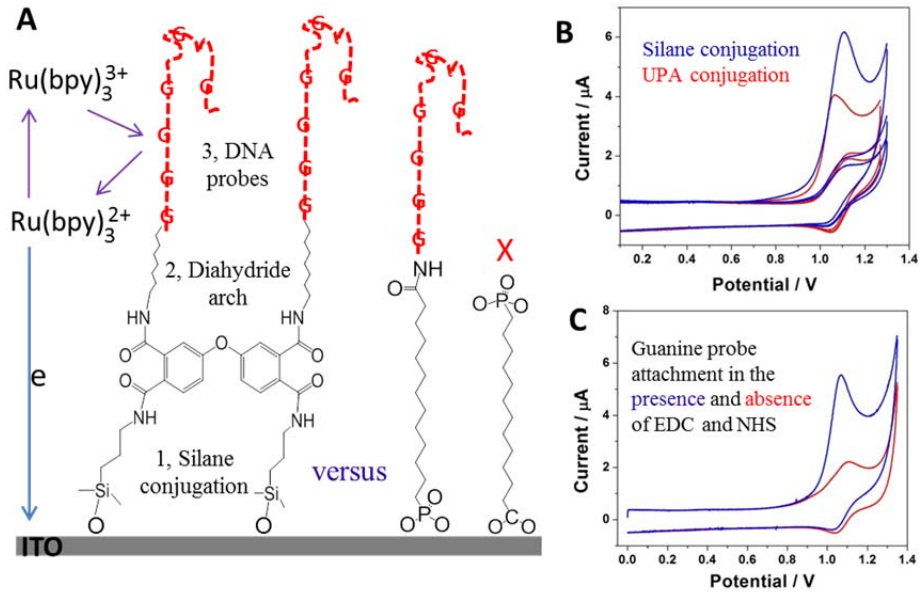

Figure 1. A) Schematic of surface chemistries of attaching single stranded DNA (guanine probe) to estimate and compare the probe density. B) Comparison of detection sensitivity between

silane and phosphonic surface chemistries, and C) the evidence of simultaneous formation of two peptide bonds and two free carboxylic acid functionalities.

Design of viral RNA fragments derived from West Nile virus. Viral RNA fragments derived from West Nile virus were generated by using reverse primer sequences (homologous to probe sequences used to detect the transcripts) and forward primers with a T7 promoter sequence at the 5' end (Figure 2). Amplicons were produced by reverse-transcribing wild-type (NY99) infectious-clone-derived West Nile virus genomic RNA with a first-strand cDNA synthesis kit (Invitrogen, Carlsbad CA) and the reverse primer, as per manufacturer's suggested reagent ratios in 25 uL reactions. The resulting cDNA was diluted 1:100 and was then used as the template in 25uL PCR reactions using a 2X PCR Master Mix (Promega, Fitchberg WI) with both the reverse and forward primers. The PCR products were then electrophoresed on a 1% agarose gel, and the appropriate amplicons excised and gel purified with agel extraction kit (Qiagen, Valencia CA). Purified amplicons were then used as templates in an *in vitro* transcription reaction using a 5X T7 Megascript kit (Ambion, Austin TX) as per manufacturer's protocol and ratios. RNA's were precipitated using lithium chloride and electrophoresed on a 1% agarose gel as well as a 6% TBE-Urea PAGE to verify expected product size.

West Nile virus has a single-stranded, positive-sense RNA genome of ~11kb in length. We designed three different inosine substituted DNA probes, specifically targeting positions at 2255, 5231, and 9917 of the viral genome. The detection sensitivity was tested by varying both probe length and target length, and compared to a synthetic RNA of 60 bases purchased from Integrated DNA Technologies, Inc. One series of vRNA sequences, targeted gene positions, and the corresponding probe sequences, are shown in Scheme 1. The probes were all purchased from Integrated DNA Technologies, Inc.

Primer	Sequence (5'-3')	Genome Position
WNV Sandia 1 R	GATCCAAAGTCCCAAGCTGTGTCTC	2255-2231
WNV San1 513bp	attatTAATACGACTCACTATAGGGagctctgcatcaagctttggctgg	1743-1769
WNV San1 993bp	attatTAATACGACTCACTATAGGGctggggcaacggctgcggactatttg	1263-1291
WNV San1 2141bp	attatTAATACGACTCACTATAGGGcccggcaagagccgggctgtc	115-138
WNV Sandia 6 R	TGTGGCAGAATCCTCCTTGTTTTAC	5231-5207
WNV San6 507bp	attatTAATACGACTCACTATAGGGcgtgatggttgaaggtgttttccac	4725-4752
WNV San6 956bp	attatTAATACGACTCACTATAGGGctggcagagcttgacattgactcc	4276-4302
WNV San6 5012bp	attatTAATACGACTCACTATAGGGccaatacgatttgtgttggctctc	220-246
WNV Sandia 7 R	GATATGCGAGCTCTGCCTACC	9917-9897
WNV San7 535 bp	attatTAATACGACTCACTATAGGGccatcattgagctcacctatcgtc	9383-9408
WNV San7 1005bp	attatTAATACGACTCACTATAGGGtgccatgtttgaagagcagaatc	8913-8938
WNV San7 5036bp	attatTAATACGACTCACTATAGGGcaggatgaggtgcagatgattgtg	4882-4908

TAN = T7 Promoter Leader ORANGE= T7 Promoter BLACK= WNV Genomic sequence

RNA Target Sequences for WNV Sandia 1R Probe:

San1 513nt:

GGGAGCTCTGCATCAAGCTTTGGCTGGAGCCATTCCTGTGGAATTTTCAAGCAACACTGTCAAGTTGACGTCGGGTCATTTGAAGTGTAGAGTGAAG
ATGGAAAAATTGCAGTTGAAGGGAACAACCTATGGCGTCTGTTCAAAGGCTTTCAAGTTTCTTGGGACTCCCGCAGACACAGGTCACGGCACTGTGG
TGTTGGAATTGCAGTACACTGGCACGGATGGACCTTGTAAAGTTCCTATCTCGTCAGTGGCTTCATTGAACGACCTAACGCCAGTGGGCAGATTGGTC
ACTGTCAACCCTTTTGTTTCAGTGGCCACGGCCAACGCTAAGGTCCTGATTGAATTGGAACCACCCTTTGGAGACTCATACATAGTGGTGGGCAGAGG
AGAACAACAGATCAATCACCATTGGCACAAGTCTGGAAGCAGCATTGGCAAAGCCTTTACAACCACCCTCAAAGGAGCGCAGAGACTAGCCGCTCTA
GGAGACACAGCTTGGGACTTTGGATC

Figure 2. Development of viral RNA fragments showing DNA primer sequences, genome position, and amplicon lengths.

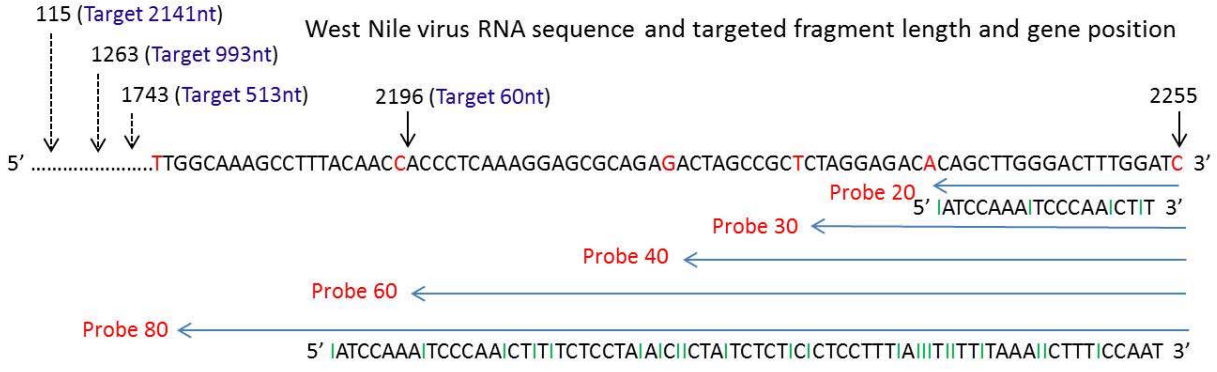

Scheme 1. The sequences of vRNA derived from West Nile virus and the inosine substituted probes. The DNA probes attached to the ITO surfaces are the reverse sequences from 5' to 3'.

Detection of RNA hybridized to inosine substituted DNA probes. All guanines in the probe are substituted by inosines in order to have very low background current from the oxidation of the probe itself. Inosine has similar binding properties as guanine but a much more positive oxidation potential. Each probe molecule has an amine at its 5' end connected through a C6 alkane chain. The DNA probe concentration in its attachment reaction was 0.1 μM. The hybridization solution was 100 mM HEPES buffer (pH 7) containing 10 mM Mg^{2+}. The target RNA concentration was tested from fM to nM range. To assure effective hybridization, the electrodes modified with DNA probes were fully immersed in the hybridization solution. The mixtures were first warmed to ~75°C for 10 min then slowly cooled to ~ 40°C and kept for another 2 hours. The electrodes were then thoroughly rinsed with HEPES buffer and water. The electrochemical test solution was 100 mM phosphate buffer (PB) containing 25 μM $Ru(bpy)_3Cl_2$. This concentration of $Ru(bpy)_3Cl_2$ was found to lead to sufficient guanine oxidation at a scan rate of ~100 mV/s. The concentration and the scan rate are compared to those found from Throp's coworkers.

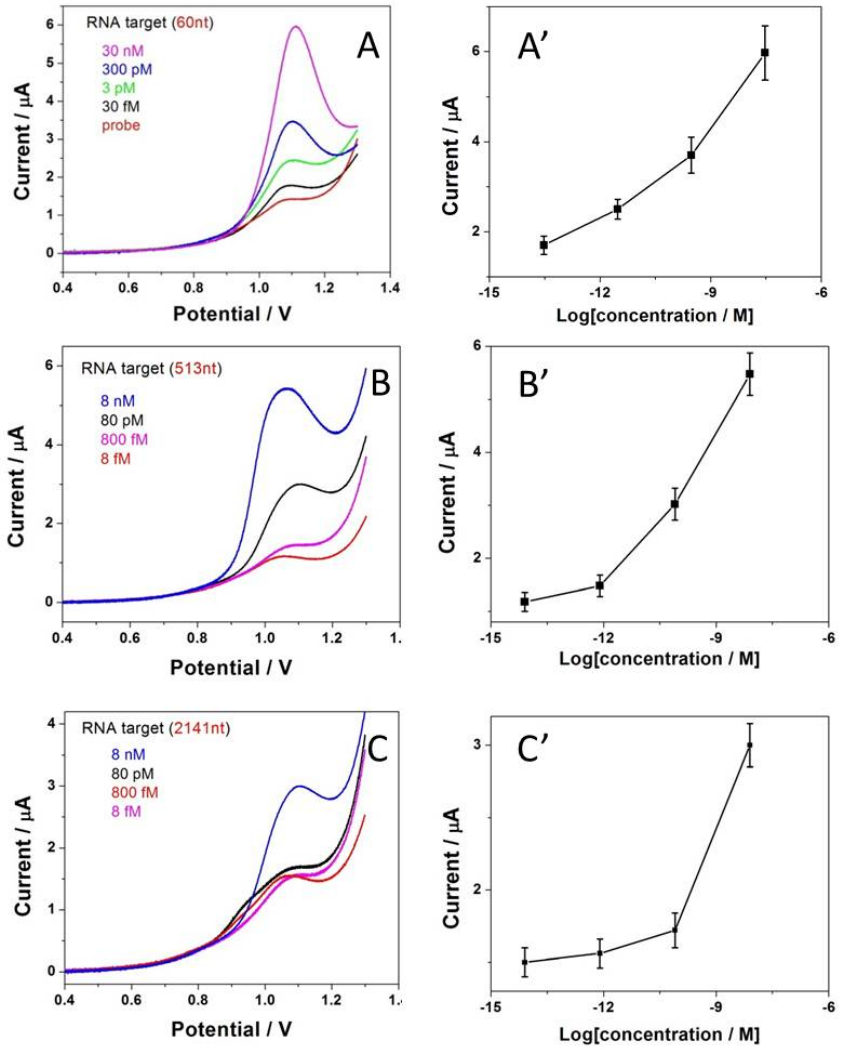

Figure 3. Electrocatalytic detection of vRNA of different sequence length: (A, A') 60 bases, (B, B') 513 bases, and (C, C') 2141 bases. The errors were determined from three ITO samples at individual concentrations.

Figure 3 summarizes the RNA detection sensitivity and limit. The DNA probe length is 30 bases. For short RNAs, such as 60 and 513 bases, the detection limit is in the fM range (Figure 1A, B). For longer RNAs, such as 993 and 2141 bases, the sensitivity is decreased to the pM range.

The sensitivity was not expected to decrease with the increase of target length. Longer sequences of vRNA having more guanine bases should lead to larger oxidation current. Such abnormal decrease in sensitivity may be due to the decrease of hybridization probability associated with the vRNA length.

Figure 4A shows the oxidation of vRNA of different sequence length at the same concentration. The hybridization protocol was the same as described above. We observed a decrease in the current with increasing lengths of vRNA. The same trend was also observed when varying the probe length (Figure 4B).

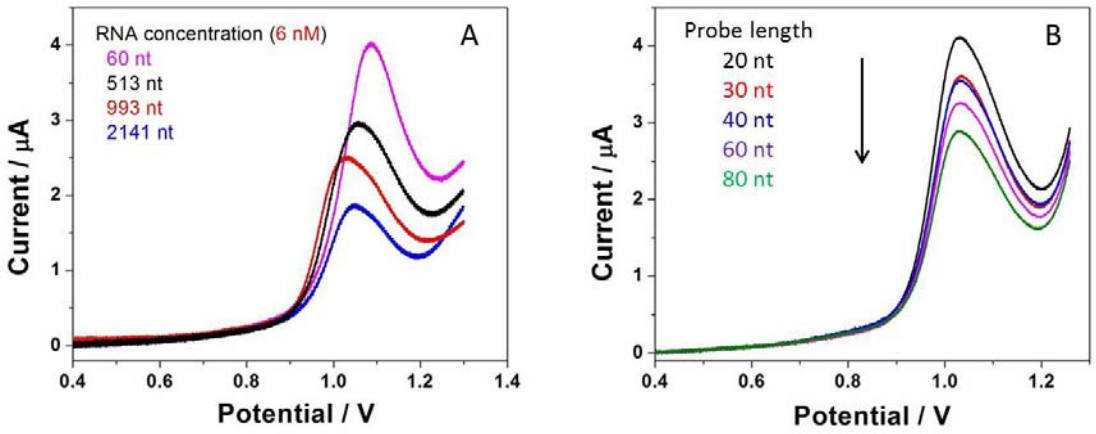

Figure 4. Sensitivity of detecting vRNA at variable target sequence length (A) and probe sequence length (B).

Why is hybridization probability decreasing with the increase of the target vRNA sequence length? First, vRNA of longer sequence normally possesses severer structural folding, so that the small portion of sequence necessary for hybridization may be deeply buried. Second, the structural folding may lead to insufficient oxidation of guanines.

AFM characterization of RNA at electrode surfaces. We have tried to apply atomic force microscopy (AFM) to examine the folding of vRNA of different sequence length attached to the ITO surface, but could not obtain single molecule resolution, mostly due to the rough surface of the ITO electrodes. Instead, we performed AFM analysis on a mica substrate with exactly the same procedures of surface modification. The atomically smooth mica would provide high lateral resolution to resolve individual RNA strands. The height of RNA strands lying on the mica surface was found to be ~ 0.5 nm (height sections in green in Figure 5). The strands were randomly distributed all over the surface with locally low and high surface coverage. Almost every individual RNA strand was found to be associated with a bright dot, which is about 3 nm in height. The other dots seen in both images of figure 5 were distributed to be about 2 nm, 1 nm,

and 0.5 nm in height. These dots of characteristic height were assumed to be due to the multiple stage of surface functionalization, an indication of the probability of each surface reaction followed at the same locations.

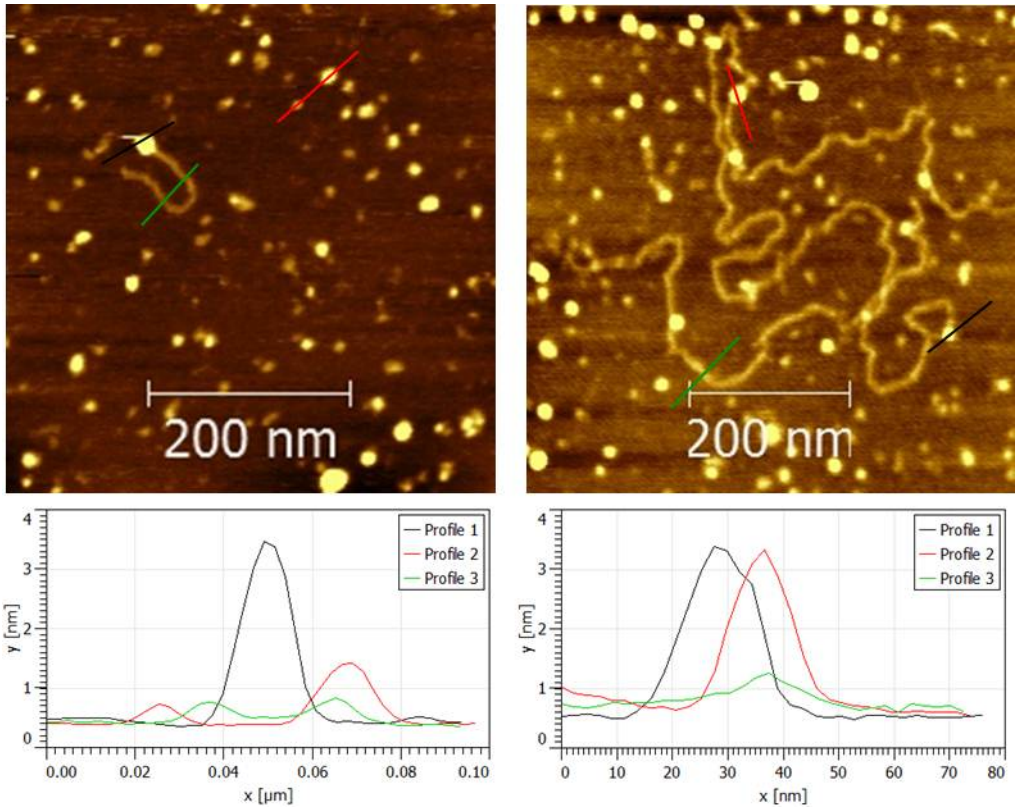

Figure 5. Representative AFM images of the surface area with very low (left) and high (right) hybridization probability. vRNA 513 was hybridized to a mica surface with the attachment of 30 base probes. The height section illustrates the multiple stage of surface modification.

The atomic smooth background of mica substrates provides a very useful measure towards multiple surface reactions. The first step of surface salinization led to dots about 0.5 nm in height, then, the dots were partially increased to about 1 nm after the second step of surface functionality. The 30 base probes appeared as clusters of ~ 2 nm in height, which is far less than the theoretical length, indicating that the probe was not stretched upwards at the surface. They were folded as clusters. Other than these clusters we did not see any features that match the probe length, ~ 10 nm (~ 0.3 nm per base)[19]. It is very clear that the surface coverage of both the probe and hybridized target vRNA is far less than a full monolayer. Even at the approximately saturated oxidation current, ~ 100 nM target vRNA concentration, the RNA surface coverage is

still ~ 5 orders of magnitude less than atomic density of a planar surface, only ~ $2x10^{10}$ molecules/cm^2 calculated from the oxidation current.

1.3. CONCLUSIONS

In summary, we have applied robust silane surface chemistry coupled with multifunctional dianhydride reactions to attach high density, stable DNA probes on ITO electrodes. Through a simple electrocatalytic redox cycle of $Ru(bpy)_3Cl_2$, we can easily obtain viral RNA detection limit at the fM to pM range. The ITO surfaces after attaching DNA probes are hydrophilic, which is necessary to prevent nonspecific binding of proteins and non-complimentary DNA or RNA. Since the surface chemistry is robust, the probes can be repeatedly used for a few times through thermal dehybridization (melting) process. The carboxylic acid terminated surfaces are stable over months so that the electrodes can be produced massively for DNA probe attachment and for further microfluidic device manufacturing (discussed in the following section). The detection of virus RNA or its fragments of hundreds and thousands of bases using a single probe is also becoming possible. The AFM imaging demonstrates the specific single RNA binding and possibly nonspecific binding of RNA aggregates.

1.4. REFERENCES

1. Heo, S; Kim, K; Christophe, R; Yoon, TY; Cho, YH, Simultaneous detection of biomolecular interactions and surface topography using photonic forcemicroscopy, Biosensors & bioelectronics **2012**, 42, 106-111.

2. Gao, AR; Lu, N; Wang, YC; Dai, PF; Li, T ; Gao, XL; Wang, YL; Fan, CH, Enhanced Sensing of Nucleic Acids with Silicon Nanowire Field Effect Transistor Biosensors, Nanolett. **2012**, 12, 5262-5268.

3. Xu, BQ; Li, XL; Xiao, XY; Sakaguchi, H; Tao, NJ, Electromechanical and conductance switching properties of single oligothiophene molecules, Nanolett. **2005**, 5, 1491-1495.

4. Lai, S; Demelas, M; Casula, G; Cosseddu, P; Barbaro, M; Bonfiglio, A. Ultralow Voltage, OTFT-Based Sensor for Label-Free DNA Detection, Adv. Mater. **2013**, 25, 103-107.

5. Wang, KM; Huang, J; Yang, XH; He, XX; Liu, JB. Recent advances in fluorescent nucleic acid probes for living cell studies, Analyst **2013**, 138, 62-71.

6. Drummond T G.; Hill, M. G.; Barton, J. K.; Electrochemical DNA sensors, Nature Biotech. **2003**, 21, 1192-1199.

7. Palecek, E. and Bartosik, M. Electrochemistry of nucleic acids, Chem. Rev. **2012**, 112, 3427-3481.

8. Wang, J.; Fernandes, J. R.; Kubota, L. T. *Anal. Chem.* **1998**, *70*, 3699-3702.

9. Wang, J.; Bollo, S.; Paz, J. L. L.; Sahlin, E.; Mukherjee, B. *Anal. Chem.* **1999**, *71*, 1919-1931.

10. Das, J; Yang, H. Enhancement of electrocatalytic activity of DNA-conjugated gold nanoparticles and its application to DNA detection. J Phys Chem C **2009**,113, 6093–6099.

11. Pheeney C. G.; Guerra, L. F.; Barton, J. K.; DNA sensing by electrocatalysis with hemoglobin, PNAS **2012**, 109, 11528-11533.

12. Pelossof G, Tel-Vered R, Elbaz J, Willner I () Amplified biosensing using the horseradish peroxidase-mimicking DNAzyme as an electrocatalyst. Anal Chem, **2010**, 82, 4396–4402.

13. Xia, F.; White, R. J.; Zuo, X.; Patterson, A.; Xiao, Y.; Kang, D.; Gong, X.; Plaxco, K. W.; Heeger, A. J. J. Am. Chem. Soc. **2010**, 132, 14346−14348.

14. Armistead, P.M.; Thorp, H.H. Anal. Chem. **2000**, 72, 3764–3770.

15. Armistead,P.M.; Thorp,H.H. Anal. Chem. **2001**, 73, 558–564.

16. Popovich, N.D.; Eckhardt, A.E.; Mikulecky, J.C.; Napier, M.E.; Thomas, R. S. Electrochemical sensor for detection of unmodified nucleic acids, Talanta **2002**, 56, 821–828.

17. Chen, F.; Huang, Z.; Tao, N. Forming single molecular junctions between indium tin oxide electrodes, Appl. Phys. Lett. **2007**, 91, 162106.

18. Napier M E; Thorp HH. Modification of electrodes with dicarboxylate self-assembled monolayers for attachment and detection of nucleic acids, Langmuir **1997**, 13, 6342-6344.

19. J Glass, G W Wertz, Different base per unit length ratios exist in single-stranded RNA and single-stranded, Nucleic Acids Res. **1980**, 8, 5739–5751.

2. Development of Prototype Electrochemical Diagnostic Platform

2.1 INTRODUCTION

Appropriate diagnostic technologies for use in outbreak settings, and at the bedside are currently lacking, as are platforms applicable to on-site medical care sites or rudimentary field laboratories and hospitals, which are neither amenable to sophisticated laboratory equipment nor to aseptic conditions. Accordingly, as part of this project we proposed to develop a robust and reliable point-of-care device for the detection of arboviruses under emergency conditions. This work would include integration of the attachment chemistries, the electrochemical bioassay, and sensing electrodes within a microfluidic diagnostic platform. Technical advantages and innovations of the designed system over current microfluidic bio-detection systems are a COTS-based MUX (MUltipleXer) electronics board intimately coupled to a custom microfluidic electrode array chip, allowing independent addressability, including activation and readout from each electrode on the array. This allows detection of multiple analytes and/or markers in each channel of the array. In addition, the demonstrated MUX was initially designed with the goal of miniaturization via an application specific integrated circuit (ASIC) approach, easing further miniaturization if required.

2.2 DEVICE DESIGN AND FABRICATION

Overall design of the detection system. Figure 1 provides a solid model and photograph of the microfluidic-based electrochemical detection system created through this project, illustrating the important features of this design. At its core, the system has a glass microscope slide with arrays of lithographically-defined microelectrodes for electrochemical signal transduction. The microelectrode slide is adhered to a plastic laminate cartridge containing laser-machined flow channels to direct fluid samples and reagents to the microelectrode arrays. There are 10 microchannels accommodating 10 microelectrode arrays. At either end of every channel, rubber o-rings are captured in the plastic laminate. These are sized to grip and seal to plastic capillaries inserted into them. One capillary, connected to an external pumping system, is used to introduce samples and reagents; the other capillary removes waste. This approach has the advantage that the two capillaries can be cheaply replaced for each channel, eliminating cross contamination.

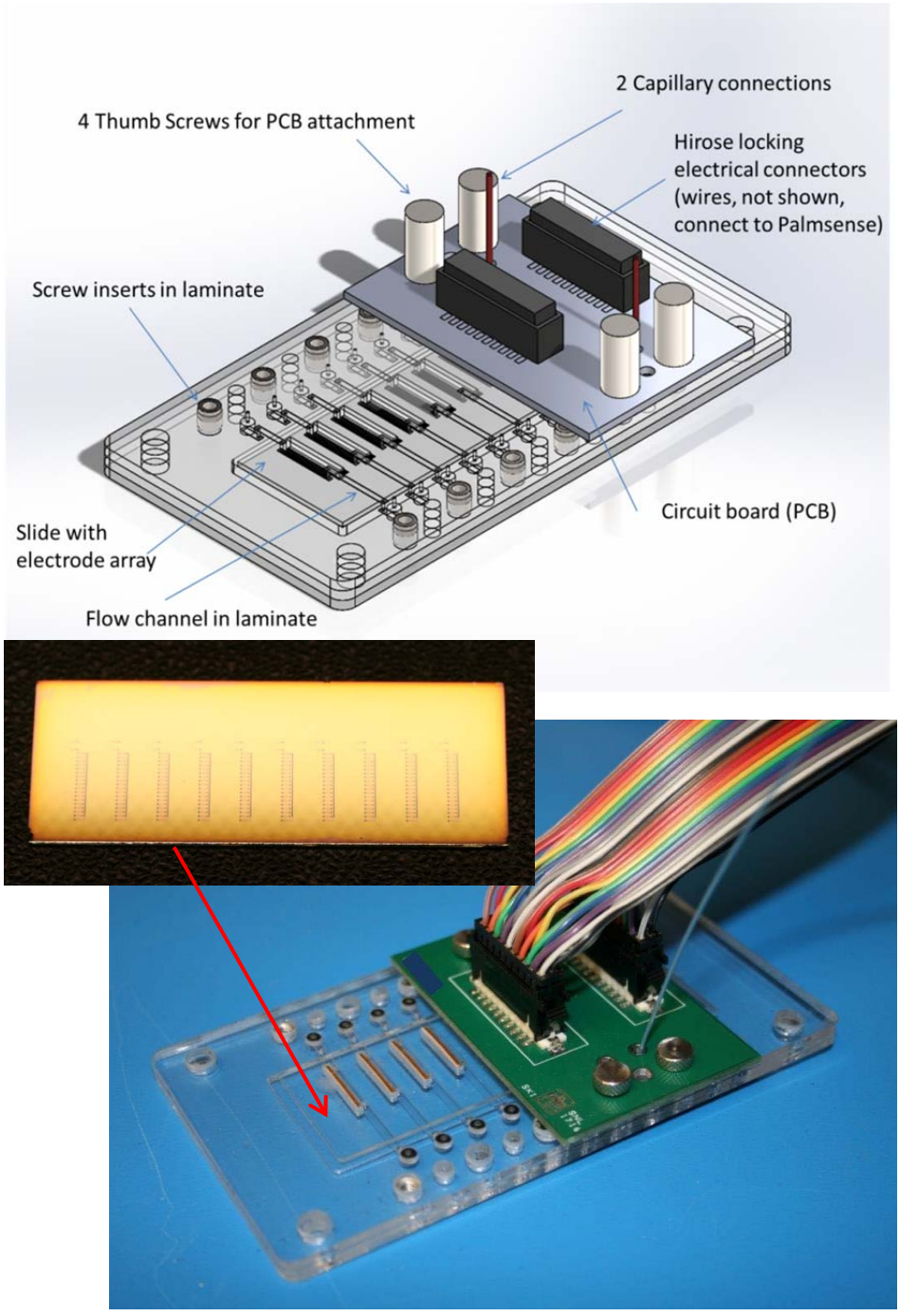

Figure 1. Solid model and photographs.

Electrical interconnections between the microelectrodes and an external potentiostat are made using z-axis elastomers, a printed circuit board (PCB) and a multi-wire cable connected to the PCB using miniature Hirose locking connectors. There are two Hirose connectors on the PCB,

allowing two microelectrode arrays to be probed before repositioning the PCB. The PCB is aligned over two rows of the cartridge using a combination of engineered mechanical positioning tolerance for gross alignment, and a novel electrical alignment method described below for fine alignment. This process aligns the microelectrode pads on the glass slide to mating pads on the underside of the PCB. The connection between these pads is made by a z-axis elastomer pressed into a rectangular well laser-machined in the laminate. The z-axis material is compressed between the slide and PCB by four 4-40 thumb screws, making electrical interconnection. The knurled thumb screws are relatively easy to install even with gloved hands. Steel inserts in the plastic laminate accept the thumb screws. Once the two microelectrode arrays are probed, the PCB is repositioned over the next two arrays, and so forth, until all 10 arrays have been utilized. The cartridge can then be discarded, but the PCB can be re-used. It should be pointed out that the spacing of the microelectrode arrays was designed to use the PCB shown in Figure 1, or alternatively a more complicated electronic multiplexing circuit (MUX) developed in a previous program (Figure 2).

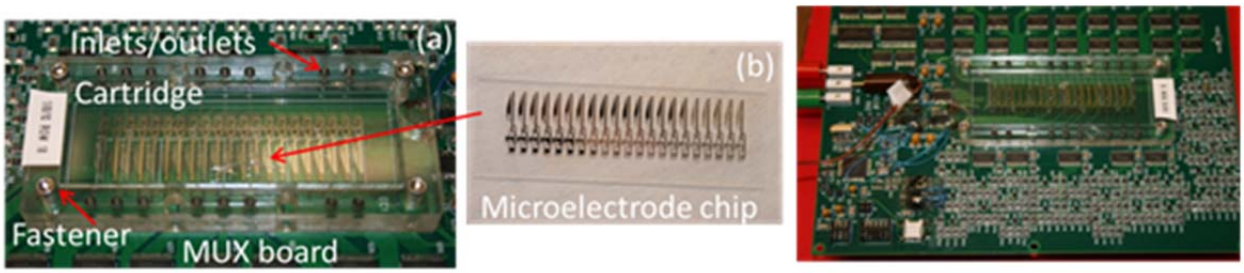

Figure 2. The new microelectrode slide chip also aligns to a previously developed MUX

Details of the slide and microelectrode arrays. There are 10 arrays, each containing 16 working electrodes, a counter, and a reference electrode. Such an arrangement would allow for a number of configurations, for example, up to 8 assays with two repeats in each of the 10 channels. The electrodes can be either indium tin oxide (ITO) or metals such as gold. The array is shown in Figure 3 with the laminate cartridge's microchannel and z-axis elastomer access well overlain. An adhesive layer on the bottom surface of the laminate cartridge seals the cartridge to the slide, separating the fluids and the electrical connections, and ensuring that biological materials never contact the exterior electrical connections.

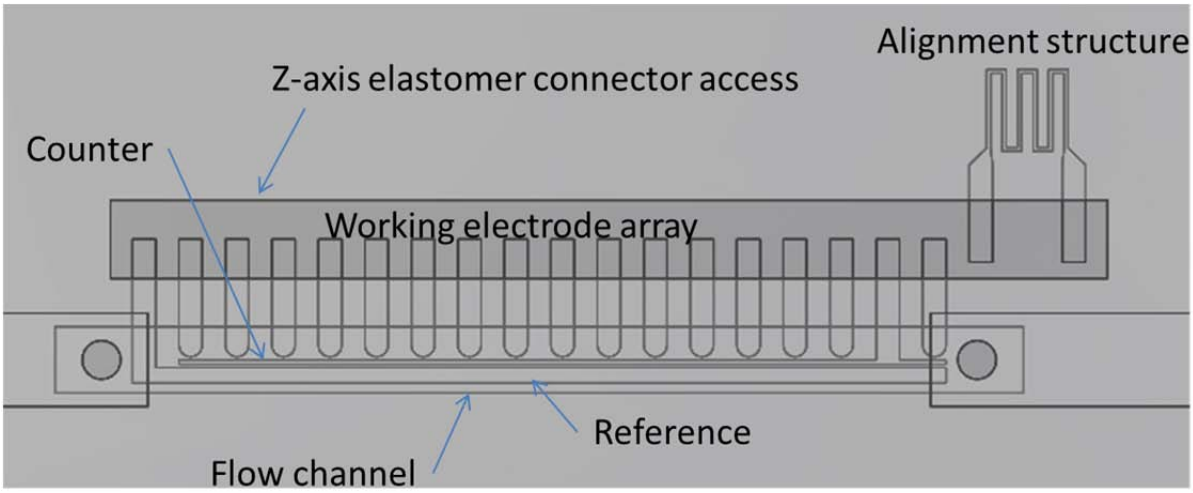

Figure 3: Close up view one analysis channels.

The slide also contains an alignment structure (Figures 3 and 4). During fine manual alignment of the PCB to the slide, electrical continuity from the alignment structure resistor is measured with a multimeter such that when its resistance is minimized, the PCB and slide are aligned. Note that the alignment structure in both rows, accessed by the PCB, can be monitored to further improve alignment.

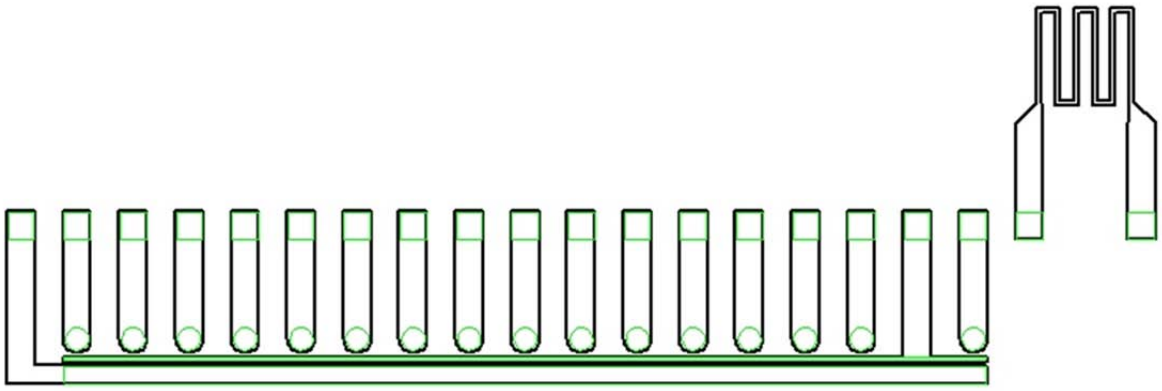

Figure 4. The open green features indicate where the dielectric overcoat is removed to expose the underlying electrode material (black lines).

Figures 4 and 5 provide more detail on the microelectrode array. In the microfabrication process, a dielectric, such as silicon nitride, silicon dioxide, or stacks of these are deposited over the entire electrode surface. The dielectric is only removed over the electrodes to precisely define the active electrode area. Again, there are 16 working electrodes, one counter and one reference

per channel. The openings in the dielectric create 250 micron diameter working electrodes, which are spaced laterally by 600 microns. This spacing allows either the MUX of Figure 2 or the PCB of Figure 1 to be used. Importantly, this spacing also allows for robotic nucleic acid probe assembly on the electrodes. For previous designs from our lab, only self-assembly was possible given much tighter lateral spacing dimensions.

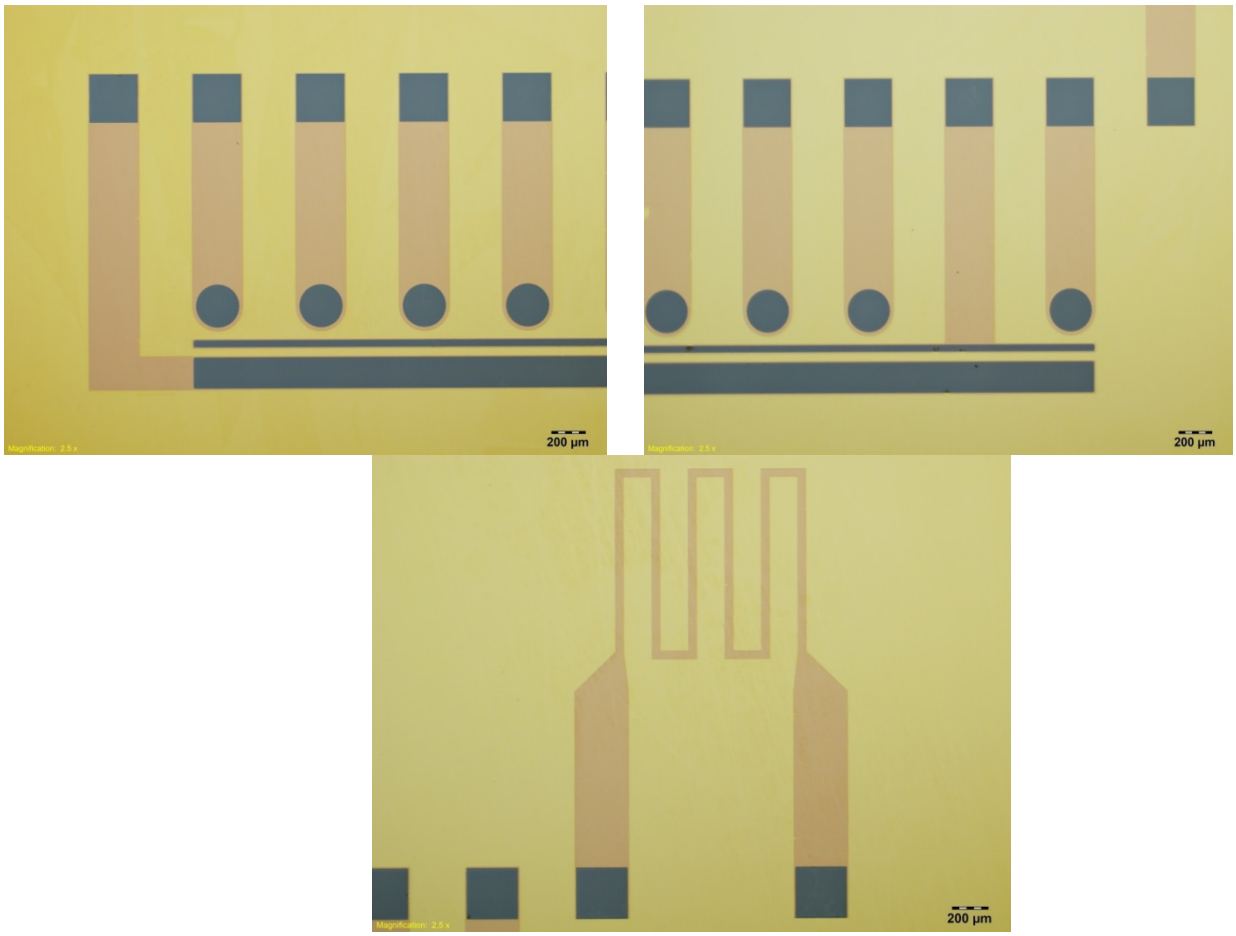

Figure 5. Photographs of three regions of the electrode slide. Blue regions are openings in the dielectric, exposing the ITO electrodes.

The advantage of our laminate-cartridge-based approach is that we can iterate rapidly, producing new cartridges within hours. Some of the parameters to be optimized include the types of electrode metallization to be used (e.g., ITO, Pt, Au) and compatible cleaning procedures for the electrodes prior to chemical functionalization. These will influence both the attachment

chemistries and the electrochemical assays to be used for detection. Optimization of channel dimensions, microelectrode geometry, flow rates and temperature through experimentation and modeling/simulation still need to be investigated; impacting optimal sensing conditions. Finally incorporating the surface chemistries and ligands within the broader microfluidics context is not without its challenges. The order of assembly of the chip, cartridge, channel passivation, attachment chemistry and ligand binding is critical. Though we have conducted preliminary studies within this microfluidic chip, it will be important to continue this work in order to develop materials and processes that are compatible with microfluidic device fabrication procedures and subsequent chemistry and biochemistry operations. The next four figures demonstrate some of the optimization experiments that have been conducted in the fluidic chip. We began with passivation of the microfluidic channels to ensure all chemistries take place at the electrode surface.

Surface passivation for patterned array electrodes. For detection of very low RNA concentrations, it is necessary to passivate the microfluidic channels, and dielectric oxides used to confine the electrode surface to avoid RNA binding besides the electrode surfaces. We have tried two passivation molecules: 2,2,2-Trichloroethyl chloroformate and 4-nitrobenzy chloroformate. The functional group of chloroformate reacts with amine groups from the surface silane modification to form a relatively hydrophobic passivation layer. Their molecular structures are shown below.

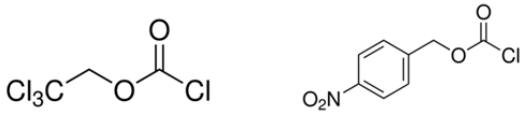

Surface reactivation selectively at the active electrode surfaces. The above passivation reaction occurs at all surfaces covered by silane modification, including the active ITO electrode arrays. To only activate the electrode for further probe attachment, the passivated electrodes were selectively reactivated through electrochemical reduction of the chloroformate molecules in methanol/LiClO4 solutions.

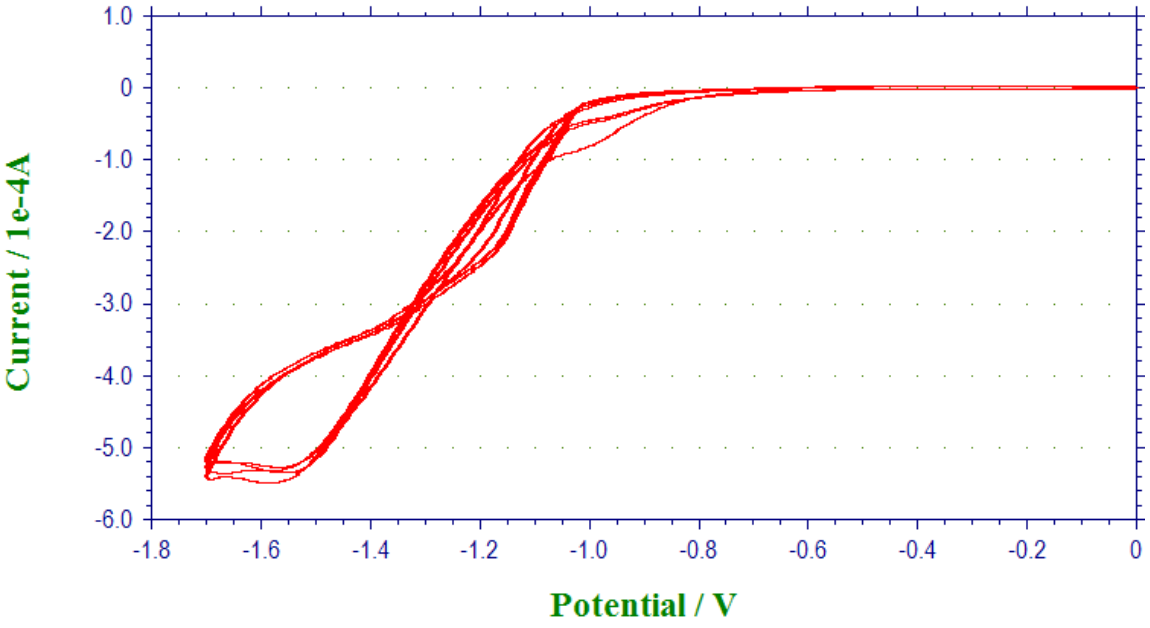

Figure 6. CV of an ITO electrode in methanol/LiClO4 solution, showing the distinct proton/Li ion reversible insertion process at the ITO electrode, which may set the potential limit for electrochemical reduction.

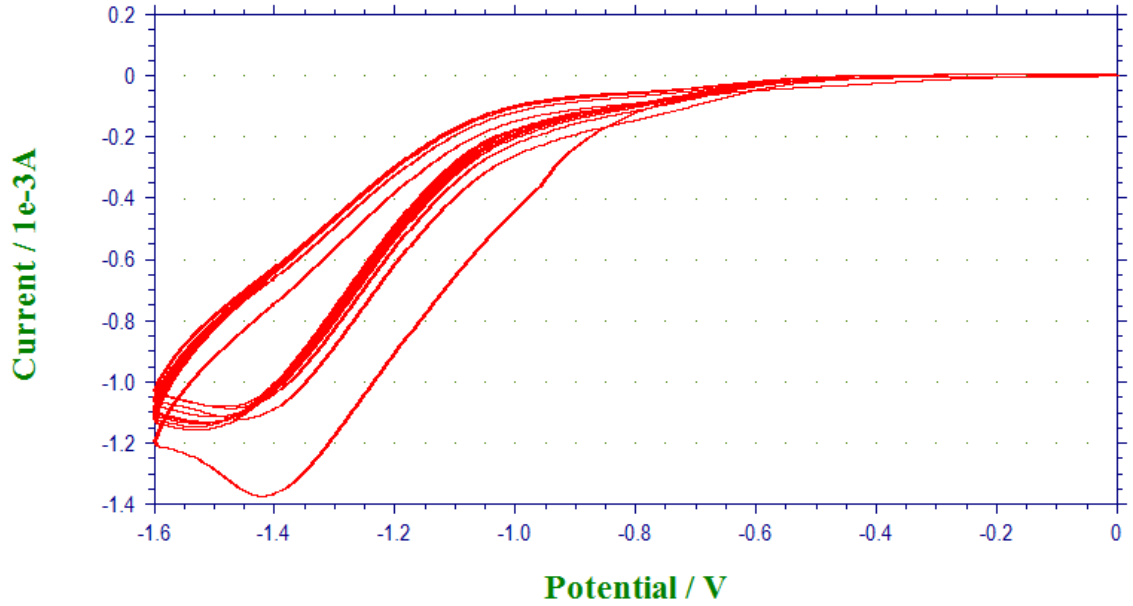

Figure 7. CV of 2,2,2-trichloroethyl chloroformate passive ITO electrode in methanol/LiClO4 solution, showing that removal of the passivation layer needs continuous potential cycling near the negative potential limit for ITO itself.

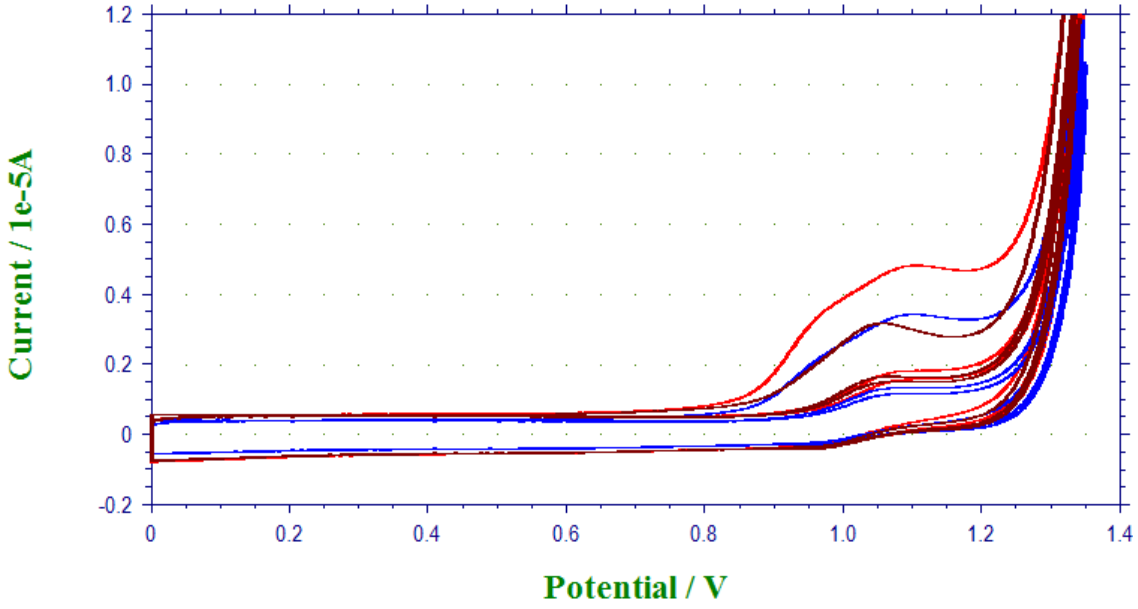

Figure 8. CV of the RNA oxidation at deactivated ITO electrodes. Deactivation process of 10 cycles between 0 and -1.6 V (red), -1.2 V (blue), and -1.0 V (dark red). This demonstrates that reduction of 2,2,2-triethyl chloroformate occurs at very negative potentials.

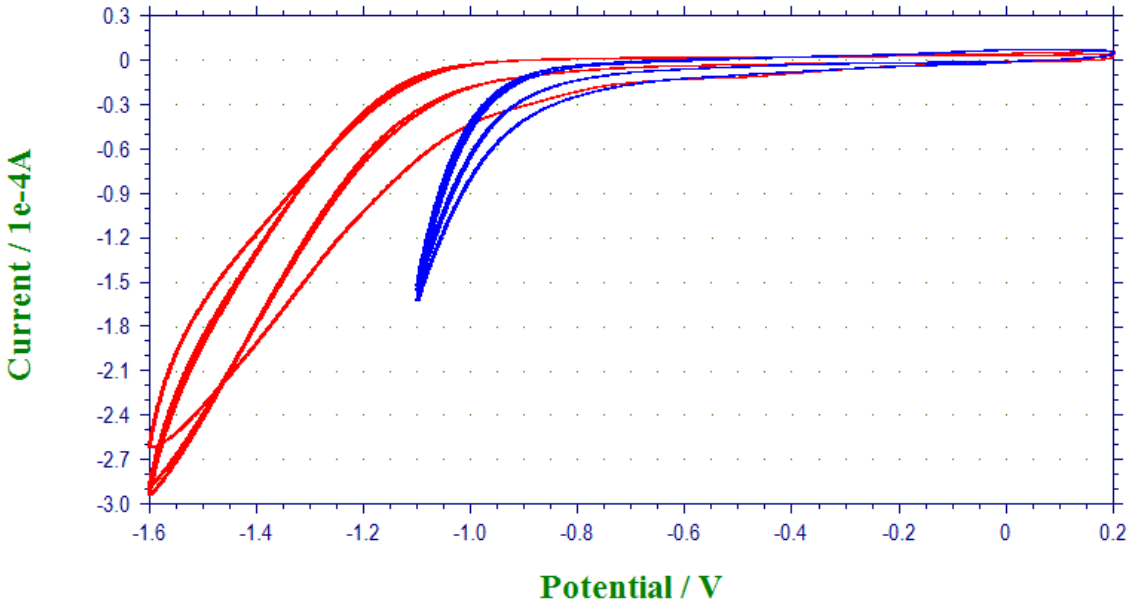

Figure 9. Comparison between electrochemical reduction of 2,2,2-triethyl chloroformate (red) and 4-nitrobenzyl chloroformate (blue).

3. Optical Detection of DNA or RNA Binding to Tethered DNA Polymerases

3.1. INTRODUCTION

Single molecule spectroscopy has been used to study the binding of primer- template DNA complexes to tethered HIV-1 reverse transcriptase (HIV RT) molecules. In this study, the 5‟ end of primer DNA was fluorescently tagged with a green quantum dot and then annealed to a longer strand of template DNA. The rates of association and dissociation were observed in terms of "on" and "off" times of the DNA duplex with a single tethered reverse transcriptase molecule. In this work, HIV RT was successfully immobilized onto an optical surface and the binding "on" and "off" times for quantum dot- primer / template complexes at concentrations of 50 pM, 75 pM, and 100 pM were measured at 25° C. The histogram for the "on" times of each concentration is a direct measure of the dissociation rate of the QD-primer / template / HIV RT complex. The histogram for the "off" times is a direct measure of the association rate of the complex. While the dissociation and association rates were determined, many factors needed verification, including the functionality of HIV RT, as well as surface homogeneity. The surface was characterized by a number of studies involving the direct observation of immobilized streptavidin and tethered HIV RT molecules as a function of increasing amounts of biotinylated BSA laid on the surface, as well as checking for non-specific binding events using labeled / unlabeled streptavidin and HIV RT antibodies.

3.2. MATERIALS, METHODS, AND RESULTS

Materials. All aqueous buffer solutions were made with NANOpure water, which was purified from dd-H_2O to a minimum resistance of 18 MΩ using a NANOpure purification system (Barnstead, USA). For the surface characterization studies, all experiments were performed in 1 mM $MgCl_2$, 4 mM KCl, and 2.5 mM Tris-HCl at pH 7.6 (1X Aqueous Buffer); components were purchased from Thermo Fisher Scientific. Bovine Serum Albumin (BSA) was purchased from Sigma Aldrich (St. Louis, MO); biotinylated BSA (bBSA) was purchased from Vector Labs (Burlingame, CA). Streptavidin and Alexa®Fluor labeled streptavidin (AF555SA), as well as neutravidin, were purchased from Invitrogen. HIV reverse transcriptase (HIV RT) was purchased from Ambion (Austin, TX) and the HIV RT monoclonal antibody was purchased from Abcam. Quantum dots with an emission maximum of 600 nm (QD600) were purchased from Ocean

NanoTech (Springdale, AK). Pegylation reagents, Methyl-PEG4-NHS and NHS-PEG4-Maleimide, were purchased from Thermo Fisher Scientific, and Dynabeads® MyOne™ Streptavidin C1 was purchased from Invitrogen. NAP-5 size exclusion columns were purchased from GE Healthcare. All custom oligos were synthesized by Eurofins MWG Operon. Borosilicate cover slips were purchased from VWR.

Cover slip preparation. All cover slips were etched and hydrophilically treated prior to use. The cover slips were etched in equal volumes of 8% H_2O_2 and 10% NH_4OH at 90º C for 20 minutes while mixing frequently. The H_2O_2 / NH_4OH mixture was decanted and cover slips were rinsed with copious amounts of NANOpure water. Next, cover slips were hydrophilically treated in equal volumes of 8% H_2O_2 and 0.5 M HCl at 90º C for 20 minutes, shaken often, and were again rinsed with copious amounts of NANOpure water. Cover slips were then dried under a stream of N_2, and then placed in a UV ozone generator for at least 30 minutes immediately prior to use.

Biotinylated BSA surface characterization. Each cover slip was first coated with a minimum layer of BSA containing different concentrations of surface available biotins. Mixing BSA with different amounts of BSA allowed the total concentration of BSA to be constant while the concentration of surface available biotin varied. To determine the amount of surface available biotins, a series of experiments were performed at 0%, 0.1%, 1%, 10%, 40%, 70%, and 100% (v / v %) bBSA / BSA with 5×10^{-6} mg / mL of AF555SA. The total concentration of bBSA plus BSA was 0.1 mg / mL for all experiments. All bBSA / BSA solutions were centrifuged at 13,200 rpm for 25 minutes at 4° C prior to use and aliquots were withdrawn from the top of the solution to reduce aggregates in the samples. 50 μL of each bBSA / BSA solution was incubated on the cover slip for 20 minutes, followed by rinsing five times with 1X Aqueous Buffer. Next, 50 μL of AF555SA was incubated for 30 minutes followed by twelve rinses with 1X Aqueous Buffer to wash off all excess (non – specifically bound) AF555SA. Finally, 50 μL of 1X Aqueous Buffer was laid down to act as the sample environment. A representation of the surface is depicted in Figure 1a. As expected, varying the amount of bBSA had an effect on the surface density of specifically bound streptavidins, see Figure 2a. Using single molecule imaging, the surface density of streptavidins could easily be determined by simply counting the number of diffraction-limited spots within the illumination field. While data above 10% bBSA had a

significant response, 1% bBSA was ideal for the remaining single molecule fluorescence studies. This surface was homogeneous with a surface coverage of 0.396 ± 0.069 molecule / μm^2.

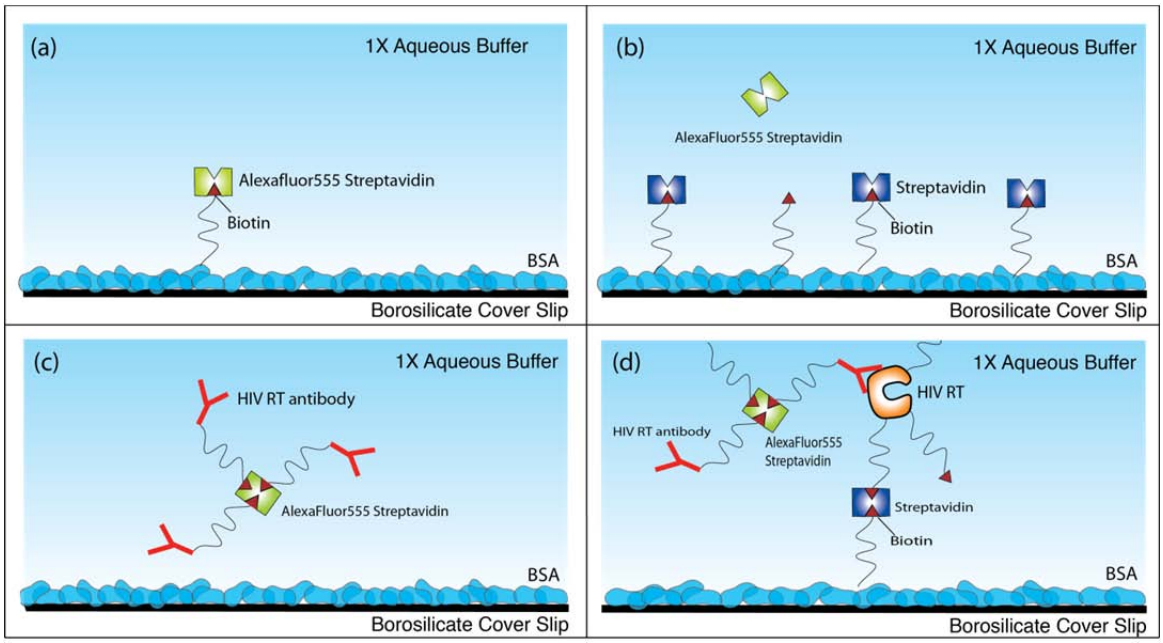

Figure 1. Surface representation of the characterization studies (a) immobilized AF555SA (5 x 10^{-6} mg / mL) on 0%, 0.1%, 1%, 10%, 40%, 70% or 100% bBSA, (b) non-specific study using unlabeled streptavidin (5 x 10^{-6} mg / mL) and AF555SA (5 x 10^{-6} mg / mL), (c) non-specific study using biotinlyate HIV RT antibody, and (d) surface available HIV RT molecules to verify counts per area from 1% bBSA from part (a).

Optimization of AF555SA incubation times. Experiments were performed to compare incubation times of AF555SA between 30 minutes, 1 hour, 4 hours, and 17 hours using 1% bBSA and 5 x 10^{-6} mg / mL AF555SA. Sample preparation was similar to that mentioned above, except incubation times for AF555SA were varied. Samples incubated for 30 minutes and at 1 hour statistically exhibited the same response though the longer incubation times led to about a 50% increase in the number of streptavidins bound to the surface (Figure 2b). A blank containing 0.1 mg / mL BSA (no surface available biotin for the AF555SA to bind) was run side–by–side for each experiment. Each blank displayed minimal non–specific binding, indicating that only specific binding events, regardless of increasing incubation times, were being observed.

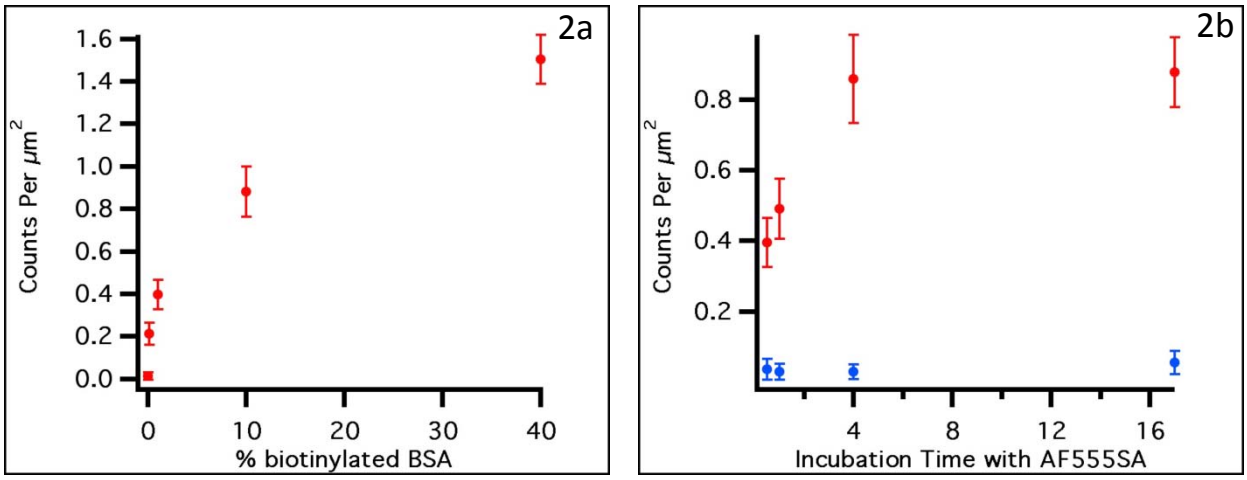

Figure 2. Counts per area of immobilized AF555SA plotted from characterization experiments at (a) 0%, 0.1%, 1%, 10%, 40% bBSA and (b) AF555SA incubation times of 0.5 hr, 1 hr, 4 hrs, and 17 hrs (red dots) on 1% bBSA surface as well as side by side blank (0.1% bBSA, no biotin) measurements (blue dots).

Quantification of streptavidin fluor (AF555SA) non–specifically bound to the surface. Experiments used to quantify the degree of non-specific binding of streptavidin were carried out using the 1% bBSA surface described above. Here 5 x 10^{-6} mg / mL of unlabeled streptavidin was used to bind to the biotin sites on the surface, effectively passivating the biotinylated surface. Next, 5 x 10^{-6} mg / mL of AF555SA was used to monitor for specific binding events of biotin sites not bound by the unlabeled streptavidin. 50 μL of unlabeled streptavidin was incubated at 1 hour and was rinsed prior to laying down 50 μL AF555SA for 1 hour. The final surrounding solution of 1X Aqueous Buffer was laid down. Depicted in Figure 1b is a representation of this surface. Non-specific binding was minimal at 0.016 ± 0.015 molecules / μm^2.

Optimization of streptavidin concentration. Based on results of the incubation time dependence studies for AF555SA to biotin, an incubation time of 1 hour was chosen for all streptavidins attached to the biotinylated surface. Using the same surface assembly as Figure 1b, the concentration of unlabeled streptavidin was varied from 5 x 10^{-3} mg / mL to 5 x 10^{-6} mg / mL using 1 hour incubation times to verify non-specific and specific binding events. AF555SA was constant at 5 x 10^{-6} mg / mL in all experiments. Minimal binding events (approximately 0 to

0.044 molecules / μm^2) of AF555SA to surface biotins as well as minimal non–specific binding were observed across all concentrations of unlabeled streptavidin.

Biotinylation of HIV RT and surface attachment chemistry. BSA passivates the surface and protects the HIV RT from strong and possibly denaturing interactions with the underlying substrate. The passivating layer is also partially biotinylated, which affords an opportunity to create BSA – biotin – streptavidin – biotin – HIV RT tethers. This set up allows HIV RT to be immobilized to a surface without perturbing it greatly. Using a Biotin-XX Microscale Protein Labeling Kit (Invitrogen), half of the amount of HIV RT was used from the vial purchased from Ambion and directly transferred into a reaction tube; a tenth volume of 1 M $NaHCO_3$ was added to the tube with HIV RT followed by the addition of 0.186 μL of 14.93 mol / μL biotin. The solution was allowed to incubate at room temperature for 20 minutes. To remove free biotin molecules, a gel resin bed was prepared in a spin filter and the biotin - HIV RT solution was placed in the center of the resin bed and centrifuged for 1 minute at 16,000 × g. The final biotin - HIV RT solution was separated into aliquots for use in individual experiments and an equal volume of glycerol was added, flash-frozen, and stored at -80° C. For the experiments, the volume of polymerase added was optimized. This kit provided approximately 3-6 biotin labels for each HIV RT molecule.

Non-Specific binding of HIV RT antibody. The next step in the assembly verification process was to determine the surface concentration of HIV RT molecules specifically bound to the surface attached streptavidin. To do this, a biotinylated HIV RT antibody was used, but the non–specific binding of this antibody had to first be determined. To do this, a 50 μL solution containing a 3:1 mole ratio of biotinylated HIV RT monoclonal antibody and AF555SA, keeping the final concentration of AF555SA as 5×10^{-6} mg / mL, was first incubated for 1 – 2 hours. The labeled antibody was then incubated for 1 hour on a BSA surface, rinsed twelve times, and the non-specific binding events were monitored using single molecule imaging. This study revealed essentially no HIV RT antibody bound to the surface (0.029 ± 0.023 molecules / μm^2). This experiment is depicted in Figure 1c.

Characterization of surface available HIV RT molecules. From the above characterization studies, 1% bBSA and 5×10^{-6} mg / mL of unlabeled streptavidin were used to tether biotinylated

HIV RT to the surface. Specifically, 50 μL of 1% bBSA was first laid down on the surface and incubated for 20 minutes, then rinsed five times with 1X Aqueous Buffer, followed by 50 μL of unlabeled streptavidin incubated for 1 hour and rinsed five times again. Next, 50 μL of biotinylated HIV RT was incubated for 1 hour and then rinsed five times. This surface was rinsed five times before a 50 μL solution of HIV RT monoclonal antibody and AF555SA premix, described previously, was added for one hour and rinsed twelve times. The final solution of 50 μL of 1X Aqueous Buffer was applied. This experiment is depicted in Figure 1d. The number of surface available HIV RT molecules was statistically identical to the number of immobilized AF555SA with a 1% bBSA surface (vide supra). This experiment was then repeated employing unlabeled neutravidin in place of unlabeled streptavidin in order to discern if the two avidin molecules were interchangeable. For the purposes of our experiments, neutravidin and streptavidin are interchangeable.

***Processive polymerization assay*.** In order to test the functionality of HIV RT attached to the optical surface, a previously published self - gated processive DNA polymerization assay was performed [1]. Briefly, this experiment uses a fluorescently labeled (Alexa®Fluor 488) nucleotide (dTTP) present at low concentrations (0.2 mM) which is necessary to trigger polymerization. When the HIV RT binds to a primer – template, a fluorescent gate base is eventually incorporated and the complex lights up at the detector. The polymerase polymerizes the DNA strand until replication of the double stranded DNA is complete and the complex goes dark again. This self – gated processive polymerization experiment was performed to test the functionality of HIV RT tethered to the optical substrate. The conditions for the experiment were the same as reported by Ortiz et al [1]. This experiment is depicted in Figure 3. In this experiment, early release was dramatically reduced and the processive polymerization was around 50% faster, suggesting a greater binding affinity for DNA and greater activity for tethered HIV RT over HIV RT non– pecifically bound to a substrate.

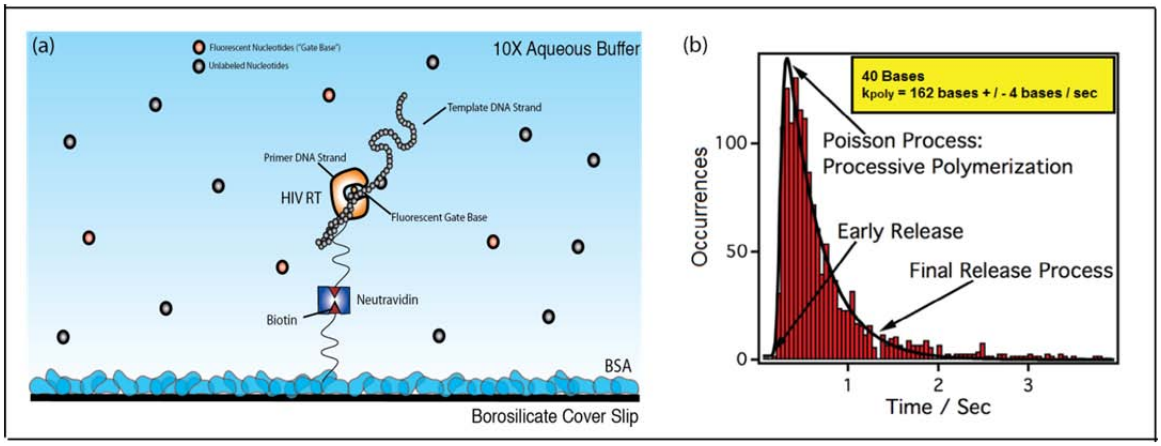

Figure 3. (a) Self gate base experiment with tethered HIV RT using a biotin – neutravidin linkage on an optical substrate. High concentrations of unlabeled nucleotide and low concentrations of labeled (Alexa®Fluor 488) nucleotide as well as primer-template DNA strands are present in solution and (b) distribution of complete replication times for HIV RT processive polymerization for a 40 base template.

Synthesis of QD-[C]$_{90}$CTGGTGGGTC. The following procedure was adapted from Ishihama and Funatsu [2]. 250 mM stock solutions of Methyl-PEG4-NHS and NHS-PEG4-Maleimide in dry DMSO were prepared prior to synthesis. A 1000 fold excess of a mixture of NHS-PEG4-Maleimide and Methyl-PEG4-NHS in a 5:95 mole ratio was reacted with 1 nmol of amino-modified quantum dots (QD600) in a microscale conical bottom vial for 1 hour under inert argon atmosphere in a total volume of 250 µL containing 50 mM sodium phosphate and 150 mM sodium chloride. After the reaction was complete, a NAP-5 column was used to remove free PEGs from the solution. The removal of free PEGs was accomplished by monitoring the fluorescent band of the pegylated QD600s eluting down the column; only one broad band was eluted and collected. All excess PEGs were contained in the column.

Prior to coupling the DNA primer to the pegylated QD, the primer was deprotected. The deprotection of the primer, 5' [ThiSS]-GACCACCCAG 3', was performed by reducing the thiol groups with 200 µL of 40 mM DTT for 16 hours in a 37º C water bath followed by filtration through a NAP-5 column to remove free DTTs. The concentration of the modified primers after filtration was determined by UV / Vis at 260 nm prior to being cross - linked to the pegylated QDs. Next, the QDs and the modified primers were cross - linked in a 1:1 mole ratio in a total volume of 780 µL of 50 mM sodium phosphate, 150 mM sodium chloride, and 10 mM EDTA

buffer for 6 hours under an inert argon atmosphere. After six hours, the reaction was quenched with 7.8 μL of 10 mM β-mercaptoethanol (BME) for 30 minutes. Free primers were removed with an Amicon Ultra-4 filter (100 kDa cutoff) in a centrifuge at 3,800 rpm and the QDs were washed with 1X PBS (Phosphate Buffered Saline, pH 7.4) buffer followed by 3X SSC (Saline – Sodium Citrate, pH 7.0) buffer for 18 minutes each.

To extract and purify only QD labeled primers, magnetic Dynabeads® MyOne™ Streptavidin C1 was used. Briefly, the QD600 labeled primers were annealed to complementary biotinylated oligonucleotides, 5'[BioTEG]-AAACTGGGTGGTC 3', using a thermocycler (BioRad MyCycler™ Thermocycler) in a 1:1 ratio. Prior to purification, the magnetic beads from the Dynabeads® MyOne™ Streptavidin C1 were washed in 2X Binding and Wash buffer (1 mM EDTA, 2.0 M NaCl, 10 mM Tris – HCl pH 7.5; buffer components from Invitrogen). The first step of this process removed free QDs over three washes using 1X B&W buffer. This was accomplished by incubating the annealed oligos with the magnetic bead solution for 12 minutes to react the biotin and streptavidin together. The separation was done using the 12-Tube Magnet kit (Qiagen) by placing the tube containing the solution of oligos and the magnetic beads against the magnet. As the magnet separated the QD600 labeled annealed oligos from the solution, a clear orange solution was observed indicative of excess unreacted QDs. The supernatant was transferred into another tube and two more washes were performed to ensure excess QDs were removed (confirmed with a UV lamp). The beads (containing QD600 labeled annealed oligos) were then re - suspended in 400 μL of 10 mM Tris - HCl buffer. QD600 labeled primers were then melted from their biotinylated oligos by placing them in a 60º C water bath for 15 minutes. Additional washes were immediately performed to remove free biotinylated oligos using 10 mM Tris - HCl buffer. The first wash provided a solution that contained virtually all the QD600 labeled primers and subsequent washes contained virtually no QD600 labeled primers. Therefore, only the first wash was retained and used in the single molecule studies. The concentration of the QD - primers was determined at 582 nm using $\varepsilon_{582\ nm}$ = 530,000 $M^{-1}cm^{-1}$. The final solution was 58.5 nM.

Preparation of QD600 - Primer / Template DNA. The QD600 - primer / template DNA duplex was formed by annealing QD600 - 5' GACCACCCAG 3' to the complementary template region of the sequence 5' $[C]_{90}$CTGGTGGGTC 3' in a 1:1 ratio. This was annealed in 1X Aqueous

Buffer using a MyCycler™ thermocycler at 75° C for 5 minutes followed by gradient cooling at 1.5° C per cycle over 35 cycles, then cooled to 25° C for 3 minutes, and finally stored at 4° C. The template length remained constant through these studies. The final concentration of the DNA / DNA duplex was 1 nM, which was further diluted for the optical studies from 50 pM to 100 pM.

Single molecule fluorescence microscopy. The instrument used in all single molecule fluorescence studies is described by Poudel et al [3]. The sample cell was specially designed for these experiments and consisted of an aluminum holder in direct contact with a copper block that acted as a large thermally controlled heat sink. The temperature was controlled with a Lakeshore A330 temperature controller and monitored with a silicon diode temperature sensor. Briefly, the microscope utilized a beam from a double cw - Nd:YAG laser (532 nm) that was passed through a 532 nm laser line filter, and a ¼ wave plate to produce a clean circularly polarized beam. The beam was then turned 90° with a broad band dielectric mirror and passed through a neutral density filter which attenuated the beam to 1 mW. This was then reflected off a dichroic mirror onto the back edge of a 1.45 N / A microscope objective (Olympus) such that the deflected beam was totally internally reflected at the glass / buffer interface. The microscope objective collected the fluorescence from the sample and passed it back through the dichroic mirror, turned 90° with a broad band dielectric mirror and the fluorescence signal was filtered through a 550 nm long pass filter (HQ550LP, Chroma Technologies Corp.) to remove scattered light prior to being imaged onto an EMCCD camera (PhotonMax 512 Model 7527-0001) with an achromatic lens. All data was captured at a time resolution of 50 ms per frame and movies were acquired with the WinView software suite (Princeton Instruments).

Photophysical studies of QD600. Like all fluorescent molecules, the QD600s have a photochemical bleaching rate under typical experimental conditions which needed to be measured. This was necessary in order to discern the DNA dissociation rate from the bleaching rate of the QD600 (vide infra). In this experiment, the QD600 labeled primer was annealed to its complementary biotinylated oligo, 5’ [BioTEG] - AAACTGGGTGGTC 3’, in a 1:1 mole ratio using a thermocycler. It was heated to 70º C for 5 minutes and incrementally decreased back down to 25º C. During the slide preparation, 50 µL of 0.1 mg / mL bBSA / BSA was applied to the surface for 30 minutes, followed by rinsing five times with 1X Aqueous Buffer. Next, 50 µL

of 0.1 mg / mL neutravidin was laid down for 30 minutes and rinsed five times with 1X Aqueous Buffer. The final 50 µL solution contained the annealed biotinlyated oligo with QD600 labeled primer. The probability distribution of "on" times was collected and the bleaching rate was determined from a histogram of fluorescent "on" times.

Binding of DNA / DNA duplexes to tethered HIV RT molecules. In these experiments, 50 µL of 0.1 mg / mL bBSA and BSA was laid down on the surface for 30 minutes, followed by rinsing five times with 1X Aqueous Buffer. Next, 50 µL of 0.1 mg / mL neutravidin was laid down for 30 minutes and rinsed five times with 1X Aqueous Buffer. Following the last rinse, 50 µL biotinylated HIV RT was laid down for 30 minutes and rinsed five times with 1X Aqueous Buffer. The final 50 µL solution contained varying concentrations of QD600 - primer / template molecules, using a template that was 100 bases long. All experiments were conducted at 298 K and the QD600 - primer / template concentrations were varied (50 pM, 75 pM, and 100 pM). The experiment is depicted in Figure 4. Dissociation rates were determined from probability distributions of "on" times using a custom Matlab program (vide infra).

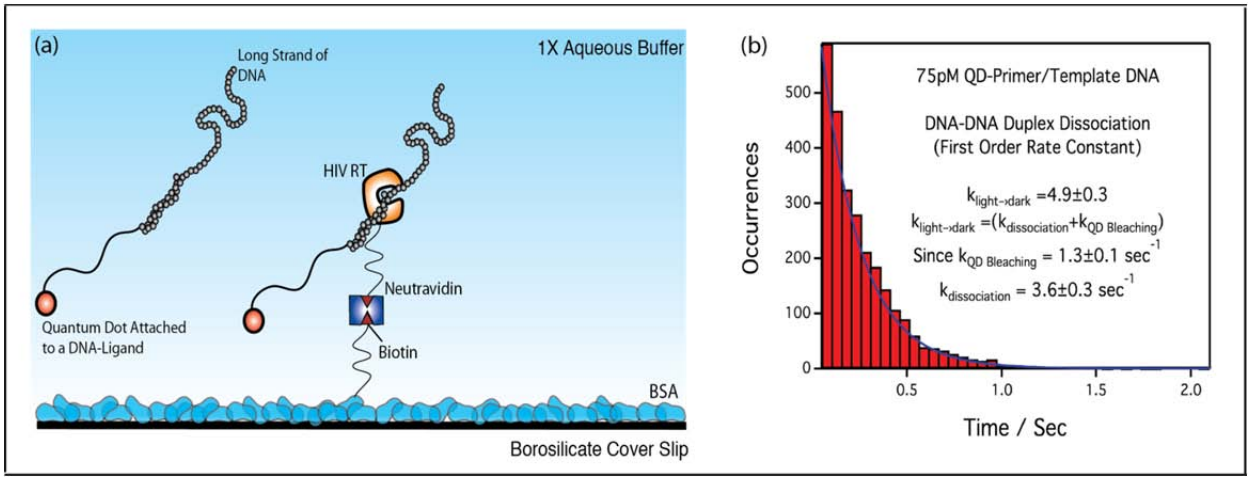

Figure 4. (a) Binding experiment using QD600 labeled primer-template strand and tethered HIV RT and (b) light to dark, or "off" rates at 75 pM QD-primer / template DNA.

3.3. DISSCUSSION

Surface characterization. Several experiments were carried out to fully understand and characterize the surface assembly. At 25° C, the components of the assembly were individually optimized for single molecule studies, including the amount of bBSA on the surface, the amount

of streptavidin used to bind with the bBSA and the time allowed for the streptavidin - biotin linkage to occur. Biotinylated HIV RT was added to the optimized surface and its activity was verified.

From these studies, it was determined that the surface density of available biotins could be adjusted from zero to 1.505 ± 0.114 molecules / μm^2, corresponding to 0% bBSA to 40% bBSA (samples at 70 and 100% bBSA were too dense to accurately quantify), as can be seen in Figure 2a. 1% bBSA, with 0.396 ± 0.069 molecules / μm^2, was ideal for the single molecule experiments performed. Longer incubation times did increase the surface density of streptavidin with a saturation density of 0.856 ± 0.104 molecules / μm^2 at 17 hours for 1% bBSA surfaces as demonstrated in Figure 2b. Also shown in Figure 2, non-specific binding events were minimal for all surface assemblies, thus the one hour incubation time for each streptavidin – biotin linkage was maintained [5,6]. The number of specifically bound streptavidins was found to be statistically identical to the number of HIV RT molecules tethered to those sites. Adding HIV RT to the optimized surface resulted in 0.423 ± 0.062 molecules / μm^2 for the unlabeled streptavidin surface and 0.438 ± 0.066 molecules / μm^2 for the unlabeled neutravidin surface, which falls within the range previously determined from the 1% bBSA surface (0.396 ± 0.069 molecules / μm^2). Overall, the streptavidin, and thus also the HIV RT, were found to give homogeneous and well – separated surfaces.

Processive polymerization assay results. For the processive polymerization experiments, modifications were made from the work done by Ortiz et al [1]. Rather than non-specifically adsorbing the HIV RT polymerase to the surface, the assembly described above was employed, thus ensuring that the polymerase was attached to the surface in a homogeneous way and free of harsh surface interactions. This drastically reduced early release rates and increased the polymerization rate from 106 ± 6 bases / s [1] to 162 ± 4 bases / s for a template with a single strand length of 40 base pairs, an increase of approximately 50%. A histogram of this data can be seen in Figure 3b. These differences (less early release and faster polymerization rate) suggest a greater binding affinity for DNA to HIV RT and higher activity of the polymerase itself.

Kinetic data: Binding of DNA / DNA duplex to tethered HIV RT molecules. When QD600 – primer / template DNA binds to surface tethered polymerases, they light up on the EMCCD

camera. A histogram of these "on" times, or the amount of time that the QD600 – primer / template DNA remains adhered to the polymerase, yields the probability distribution which reflects both the rate at which DNA leaves the HIV RT and the photochemical bleaching rate of the quantum dot. These parallel first order reactions should give an overall distribution that is also first order with an overall rate that is the sum of the DNA dissociation rate and the photochemical bleaching rate. In a separate experiment, the bleaching rate was determined to be $1.3 \pm 0.1\ s^{-1}$. The DNA dissociation rates were determined to be $3.5 \pm 0.3\ s^{-1}$. Data is shown in Figure 4.

Application to microfluidic systems. The entire experimental setup and surface chemistry was adapted and used with a microfluidic flow cell for inline RNA and DNA detection. The surface chemistry and sample conditions were identical that that described above, but a new, compact instrument was designed and constructed. This instrument is depicted in Figure 5. Briefly, a doubled Nd:YAG laser (Sapphire, Coherent Inc.) was attenuated with neutral density filters to 200 μW then directed with a periscope to a prism that was place in contact with a microfluidic chip via index matching fluid. The microfluidic chip was pretreated in the same manner as described for the glass coverslips and contained the sample. The incident angle of the laser was adjusted with the periscope such that the laser underwent total internal reflection at the interface between the microfluidic chip and the aqueous sample solution. The depth of the evanescent field setup by the total internal refection could be further adjusted with the periscope. The emitted fluorescence from RNA/DNA duplexes from the sample (the DNA severed as the fluorescent probe for the RNA) was then collected with an Olympus 100x (1.3 NA) microscope objective attached to a three dimensional optical stage allowing for the sampling of any channel contained within the chip. The light was then passed through a cutoff filter (549 nm low pass), collected by a fiber coupler, and launched into a 100 μm fiber (the fiber also served as a pinhole; i.e. confocal arrangement). The fiber was then connected to a single photon counting avalanche photodiode (PerkinElmer SPCM-AQR-16; darcounts = 25 counts per second). The output (TTL pulses) of the APD was fed to a national instruments interface board (NI-BNC2121) driven by an Agilent function generator (33220A) and interfaced to a computer. The entire system, including the microfluidics, has been tested.

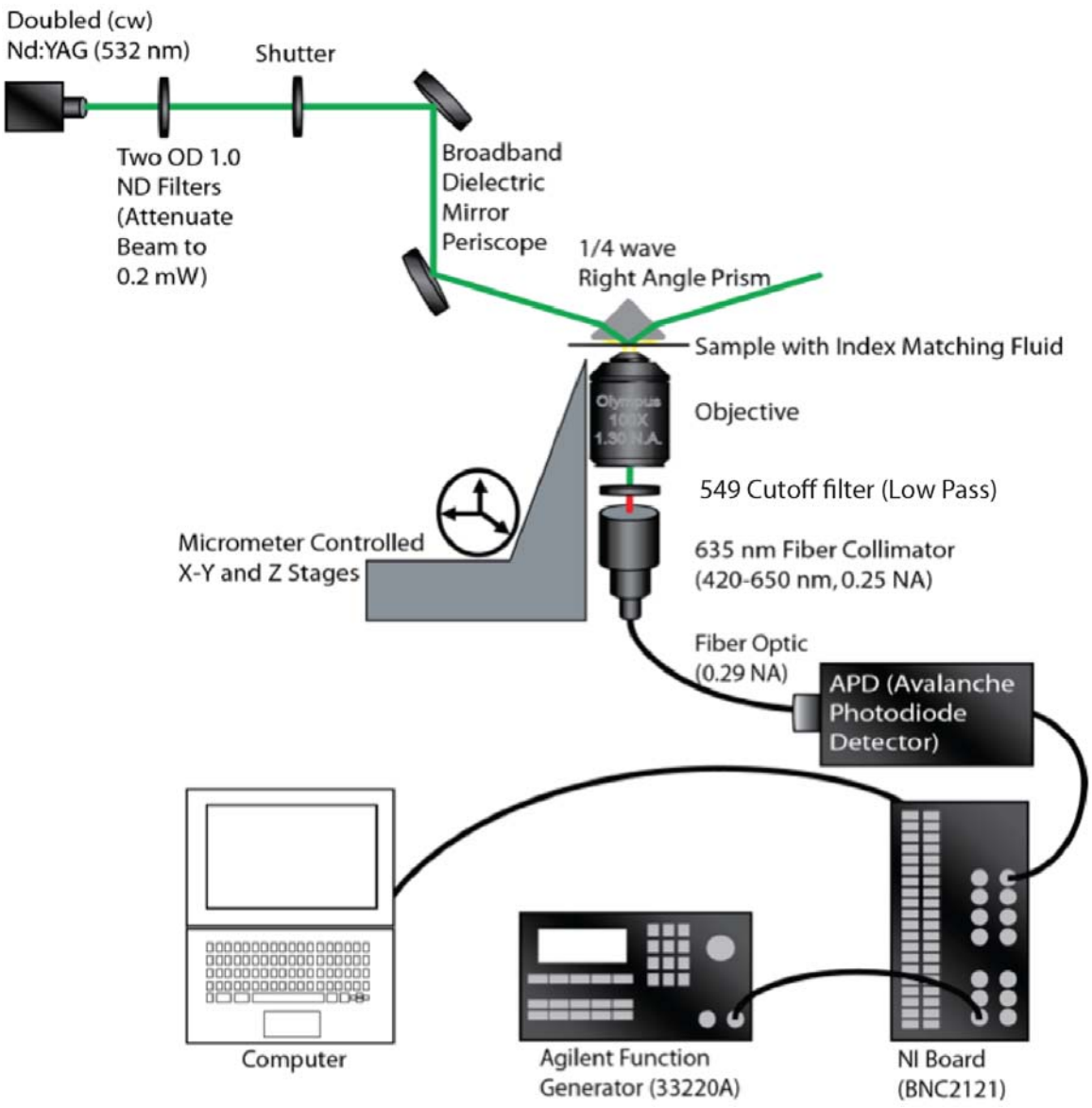

Figure 5. Microscope constructed at SNL for use with microfluidic systems.

3.4. CONCLUSIONS

The results acquired from the binding studies using QD600 as a fluorescent label for the DNA / DNA duplex demonstrates what the scientific potential of single molecule imaging brings to the detection of DNA at a bio-functionalize interface. While ensemble methods would typically mask details surrounding the dynamics of complex biological systems, single molecule methods have proved to be advantageous in these studies and should provide greater scientific detail than is currently available. One of the major advantages of using single molecule methods are that

inactive polymerases do not contribute to sources of error since they would not be visible nor would they bind to DNA / DNA duplexes. Another advantage is that probability distributions of "on" and "off" times can only be generated from single molecule experiments rather than an average from an ensemble method. While single molecule methods were utilized to study DNA binding to tethered Polymerase molecules as well as dynamical fluctuations from photophysics and photobleaching of the fluorescent probes, it can be adapted into new complex systems to investigate protein folding, enzymatic fluctuations, DNA sequencing, and many others.

In the single color experiments, dissociation rates were determined for three different concentrations of QD-DNA / DNA duplexes at 50 pM, 75 pM, and 100 pM. As expected, the dissociation rates were independent of concentration and measured to be $3.3 \pm 0.3\ s^{-1}$, $3.6 \pm 0.1\ s^{-1}$, and $3.5 \pm 0.1\ s^{-1}$, respectively. These dissociation rates are consistent with earlier studies by Ortiz et al [1].

Finally the experiment was redesigned and adapted for use with a microfluidic sample cell. This was accomplished by the construction of a custom made compact inverted confocal microscope with 532 nm evanescent laser excitation and APD detection. The system is capable of single molecule detection and was successfully tested with the microfluidic platform.

3.5. REFERENCES

1. Ortiz, T.P., et al., *Stepping Statistics of Single HIV-1 Reverse Transcriptase Molecules during DNA Polymerization.* Journal of Physical Chemistry B, 2005. **109**(33): p. 16127-16131.
2. Ishihama, Y. and T. Funatsu, *Single molecule tracking of quantum dot-labeled mRNAs in a cell nucleus.* Biochemical and Biophysical Research Communications, 2009. **381**(1): p. 33-38.
3. Poudel, K.R., D.J. Keller, and J.A. Brozik, *Single Particle Tracking Reveals Corralling of a Transmembrane Protein in a Double-Cushioned Lipid Bilayer Assembly.* Langmuir. **27**(1): p. 320-327.
4. Kati, W.M., et al., *Mechanism and fidelity of HIV reverse transcriptase.* Journal of Biological Chemistry, 1992. **267**(36): p. 25988-25997.
5. Ausubel, F.A., Brent, R., Kingston, R.E., Moore, D.D., Seidman, J.G., Smith, J.A., and Struhl, K. (eds.). 1999. *Current Protocols in Molecular Biology*. John Wiley & Sons, New York.
6. Johnson, I., M.T.Z. Spence. *Molecular Probes Handbook, A Guide to Fluorescent Probes and Labeling Technologies*. 11th Edition. Invitrogen Molecular Probes.

DISTRIBUTION

1	MS0899	Technical Library	9536 (electronic copy)
1	MS0359	D. Chavez, LDRD Office	1911


Sandia National Laboratories